

Study on MIMO-OFDM Configurations for Integrated Sensing and Communication Systems

Oscar González Fresno, María Julia Fernández-Getino García (Tutor)

Universidad Carlos III de Madrid, Spain

September, 2025

Abstract—This work investigates Multiple-Input Multiple-Output (MIMO) Orthogonal Frequency Division Multiplexing (OFDM) as a baseline for integrated Sensing and Communication (ISAC) in Sixth-Generation (6G) networks through MATLAB-based simulations. The study evaluates Bit Error Rate (BER), range, and Doppler resolution under different system configurations, including variations in the number of subcarriers, subcarrier spacing, antenna array size, and pilot allocation strategies. These configurations provide a framework to analyze the trade-offs between communication reliability and sensing accuracy in future Sixth-Generation (6G) systems.

Index Terms—ISAC, MIMO, OFDM, BER, range resolution, Doppler resolution, MATLAB simulation

I. INTRODUCTION

THE convergence of sensing and communication, commonly referred to as Integrated Sensing and Communication (ISAC), is emerging as a cornerstone for future 6G networks [1], [2]. By enabling the joint use of spectrum, hardware, and signal processing resources, ISAC systems can simultaneously deliver high-capacity data transmission and precise environmental awareness. Among the candidate waveforms for ISAC [3], Orthogonal Frequency Division Multiplexing (OFDM) stands out due to its extensive deployment in legacy and current communication standards, including 4G LTE and 5G NR [4], [5]. Its maturity, well-defined standards, and proven interoperability with existing infrastructure make it a cost-effective and practical platform for integrating sensing functionalities [6].

From a physical layer perspective, OFDM offers inherent resilience to multipath propagation through its use of narrowband subcarriers and Cyclic Prefixes (CPs), thereby improving robustness in challenging wireless channels [7]. These properties facilitate its extension to joint sensing tasks without significant modifications to transceiver architectures, reducing both implementation complexity and deployment costs. In particular, combining OFDM with Multiple-Input Multiple-Output (MIMO) arrays enhances spatial resolution, enabling accurate estimation of parameters such as target range, velocity, and angle of arrival [8]–[10].

This work investigates a MIMO OFDM ISAC system implemented in MATLAB [11], evaluating its performance under various configurations. Key performance indicators, including Bit Error Rate (BER), range resolution, and Doppler resolution, are analyzed for different system setups. The original code was refactored into separate methods and auxiliary functions to improve readability and maintainability [12].

Acceleration techniques such as parallel vectorization and GPU processing were tested but could not be implemented [13], [14], as the main computational bottlenecks resided in MATLAB built-in functions that could not be modified and were not well-suited for these optimizations.

The remainder of this paper is organized as follows. Section II introduces the system model and outlines the OFDM-based framework for joint communication and sensing. Section III details the baseline simulation setup. Section IV presents the results for the reference configuration, while Section V examines the impact of parameter variations. Finally, Section VI summarizes the findings and discusses directions for future research.

II. SYSTEM MODEL

The baseline configuration analyzed in this work follows the setup presented in [11]. The system considered is a MIMO OFDM communication platform operating at a carrier frequency of 6 GHz and occupying a total bandwidth of 100 MHz.

The propagation environment between transmitter and receiver contains multiple scatterers, which serve a dual role: they enable spatial multiplexing for MIMO communications and act as radar targets for the sensing functionality. Scatterers are located at distances not exceeding 300 m from the transmitter, with relative velocities bounded by 50 m/s, corresponding to 180 km/h.

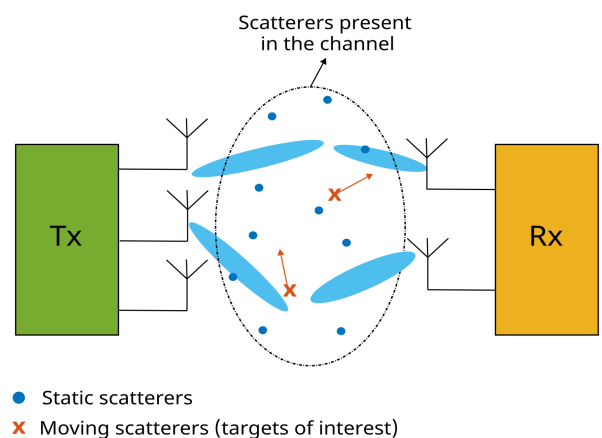


Fig. 1. System model architecture

Fig. 1 shows a scheme of the system model, illustrating the MIMO transmitters and receivers and a channel with multiple

scatterers, including both static and moving ones. The scenario assumes static transmitter and receiver nodes, with three moving scatterers representing the targets of interest (Fig. 2). These targets contribute to a rich multipath environment, enabling the simultaneous assessment of communication performance and radar-based sensing accuracy.

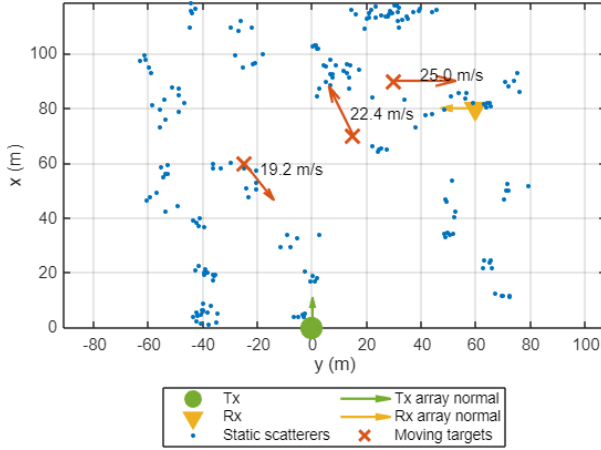


Fig. 2. ISAC scenario with static scatterers and moving targets

The system parameters are selected to support integrated sensing and communication in a realistic and dynamic propagation setting, while exploiting the spatial diversity offered by MIMO antenna arrays.

TABLE I
DEFAULT SYSTEM PARAMETERS

Description	Value
Carrier frequency	6 GHz
System bandwidth	100 MHz
Number of OFDM subcarriers	2048
Number of data streams	2
Number of transmitted OFDM frames	24
Modulation order (bits/symbol)	6
Peak transmit power	1 W
Receiver noise figure	3 dB
Reference temperature	290 K
Number of transmit antennas	8
Number of receive antennas	8

Table I presents the default parameters for the MIMO OFDM configuration. Table II lists the scenario configuration values, including the locations, orientations, and velocities of antennas and targets, as well as the maximum values for range and velocity and the number of scatterers.

A. OFDM Signal

The adopted OFDM resource grid for one transmit antenna is shown in Fig. 3. The grid includes data symbols, pilot symbols, and empty resource elements.

Each transmission begins with a preamble, which is exploited at the receiver to obtain the initial channel estimate, followed by OFDM frames divided into subframes. Subframe A is dedicated exclusively to data symbols, whereas Subframe B carries both data symbols and pilots, thereby enabling dual-purpose transmission for communication and sensing.

TABLE II
SCENARIO PARAMETERS FOR THE CONFIGURATION IN FIG. 2

Description	Value
Transmitter position	(0, 0, 0) m
Receiver position	(80, 60, 0) m
Transmitter orientation	Identity matrix
Receiver orientation	Rotation around Z-axis by -90°
Maximum Tx-Rx path length	300 m
Maximum target velocity	50 m/s
Target positions	$\begin{bmatrix} 60 & 70 & 90 \\ -25 & 15 & 30 \\ 0 & 0 & 0 \end{bmatrix}$ m
Target velocities	$\begin{bmatrix} -15 & 20 & 0 \\ 12 & -10 & 25 \\ 0 & 0 & 0 \end{bmatrix}$ m/s
Region of interest	[0, 120] × [-80, 80] m
Number of scatterers	200

To avoid inter-antenna interference, the preamble sequences are orthogonalized in the frequency domain by assigning distinct subcarriers to each transmit antenna. For channel tracking, pilot symbols are placed according to different pseudorandom binary maximum length sequences per antenna.

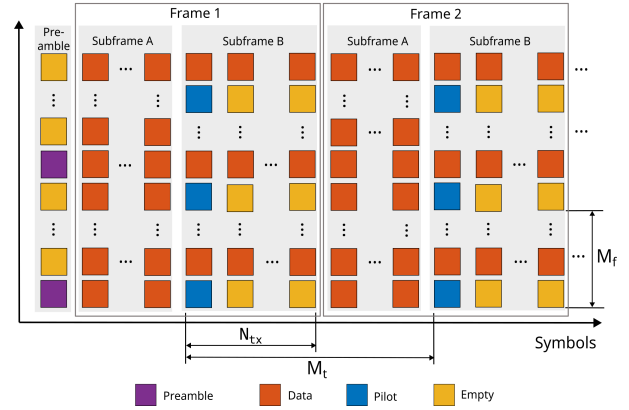


Fig. 3. OFDM resource grid structure

The system employs $N_{\text{sub}} = 2048$ equally spaced subcarriers. The subcarrier spacing is given by the ratio of total bandwidth to the number of subcarriers, and the OFDM symbol duration is the reciprocal of this spacing. Guard bands are inserted to mitigate spectral leakage [11].

A Cyclic Prefix is added to each symbol to eliminate inter-symbol and inter-carrier interference [15], [16]. The CP duration is set according to the maximum path length:

$$T_{\text{cp}} = \frac{R_{\max}}{c}, \quad (1)$$

where c is the speed of light. The Cyclic Prefix length is then converted to samples and adjusted to have an integer number of samples based on the system sampling rate.

The total OFDM symbol duration, including the CP, is:

$$T_{\text{symbol}} = T_{\text{ofdm}} + T_{\text{cp}}, \quad (2)$$

and the corresponding symbol length in samples is:

$$L_{\text{symbol}} = N_{\text{sub}} + L_{\text{cp}}. \quad (3)$$

To avoid spectral leakage from systems operating in adjacent frequency bands, a portion of the subcarriers is reserved

as guard bands. Consequently, the number of active subcarriers is given by:

$$N_{\text{sub}}^{\text{act}} = N_{\text{sub}} - N_{\text{gb}}, \quad (4)$$

where N_{gb} denotes the number of guard-band subcarriers.

Pilot symbols on Subframe B are used for both channel estimation and radar sensing. The maximum pilot spacing in time and frequency is constrained by the Doppler shift and delay spread [17]:

$$M_t \leq \frac{1}{2f_D T_{\text{symbol}}}, \quad M_f \leq \frac{1}{2\Delta_f \tau_{\text{max}}}, \quad (5)$$

where f_D is the maximum Doppler frequency and Δ_f the subcarrier spacing.

M_t and M_f are, respectively, the Doppler and range sampling parameters. The pilots used for channel estimation must be transmitted once per frame; therefore, the frame length is set equal to M_t . Each transmit antenna sends its pilots in a separate OFDM symbol to avoid interference. Consequently, the length of subframe B, which carries the pilots, is equal to the number of transmit antennas, while the remaining symbols in the frame belong to subframe A.

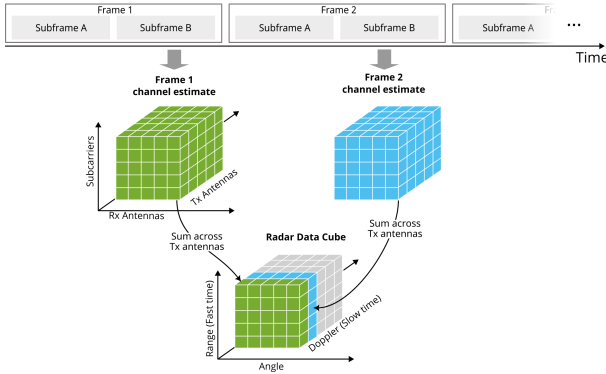


Fig. 4. Radar data cube construction

A new channel matrix estimate is obtained every M_t symbols, with dimensions $N_{\text{sub}} \times N_{\text{tx}} \times N_{\text{rx}}$. To construct the radar data cube, the channel estimates are first combined across transmit antennas, resulting in matrices of size $N_{\text{sub}} \times N_{\text{rx}}$. These matrices are then stacked over successive frames, yielding a three-dimensional array of size $N_{\text{sub}} \times N_{\text{rx}} \times N_{\text{frame}}$, where N_{frame} denotes the number of recorded frames. After mapping each dimension to its physical domain—subcarriers to *range*, receive antennas to *angle*, and frames to *Doppler*—the resulting structure corresponds to the radar data cube illustrated in Fig. 4.

B. Sensing

The sensing operation relies on extracting Doppler and delay shifts from the channel response. These are expressed as:

$$\tau_i = \frac{l_i}{M\Delta f}, \quad v_i = \frac{k_i}{NT}, \quad (6)$$

where l_i and k_i are the normalized delay and Doppler indices, $\Delta f = 1/T$ is the subcarrier spacing, M is the number of

delay bins, and N is the number of Doppler bins [18]. The channel is assumed underspread [19], satisfying:

$$l_{\text{max}} < M, \quad -\frac{N}{2} \leq k_i < \frac{N}{2}. \quad (7)$$

These indices map to physical range R and velocity V as:

$$R = \frac{c}{2}\tau_i, \quad V = \frac{c}{f_0}v_i, \quad (8)$$

where f_0 is the carrier frequency. This relationship allows the system to estimate the distance and speed of objects from the measured delay and Doppler shifts.

Sensing metrics are computed using built-in functions that produce a heatmap of moving scatterers and a range–Doppler response. The process begins with an FFT applied over the slow-time dimension, followed by nulling the DC component to suppress static scatterers.

III. SIMULATION SCHEME

The simulation framework developed in this work follows a structured execution flow to evaluate the performance of a MIMO–OFDM ISAC system. Each principal stage is described in the following subsections.

A. System Initialization

The simulation begins with the execution of the `main.m` script, which loads configuration parameters from a CSV file. These parameters include system and scenario definitions, along with visualization and result storage options. For each configuration specified in the CSV file, the simulation is executed through the `run_isac_simulation` function.

B. System and Scenario Configuration

The `configureSystem` function establishes the main system parameters, including the communication elements (antenna array geometry, transmitter and receiver configurations), waveform characteristics, and settings for figure generation. The `configureScenario` function defines the simulation environment by specifying transmitter and receiver locations, target positions and velocities, and the placement of static scatterers. Random reflection coefficients are assigned to each target and scatterer to emulate realistic propagation conditions. MATLAB’s Phased Array System Toolbox is employed at this stage to generate the communication elements and to model the MIMO scattering channel.

C. OFDM Parameterization and Channel Estimation

OFDM parameters, including subcarrier spacing, cyclic prefix length, Doppler and range resolutions, and frame length, are configured at this stage. An initial channel estimate is obtained using pilot-based preambles. The received signal is demodulated, and the channel matrix is estimated to determine the precoding and combining weights required for subsequent data transmission.

D. Data Transmission and Reception

Multiple OFDM frames are transmitted through the simulated channel. For each frame, binary payloads are generated and modulated for two subframes. The modulated waveform propagates through the channel, with target positions and velocities updated at every symbol interval to reflect motion dynamics. The received signals are then separated into subframes for further baseband processing.

E. Performance Evaluation

The received subframes are demodulated to recover the transmitted bit streams, and the BER is computed for each frame. The results are saved in text files, such as `BER_results.txt`, and visualizations, including constellation diagrams, are produced when the visualization option is enabled.

F. Radar Data Processing

Finally, the radar data cube generated during signal reception is processed to extract sensing metrics such as range and Doppler information. This stage enables the assessment of the dual-functionality of the ISAC system, combining wireless communication and radar-based sensing capabilities.

This modular and parameterized design allows for flexible experimentation with different antenna configurations, propagation environments, and system parameters, enabling a comprehensive performance analysis under diverse operational conditions. The objective of this refactoring was not only to facilitate the execution of multiple configurations, but also to apply acceleration techniques to specific parts of the code. However, these optimizations could not be achieved due to constraints imposed by MATLAB's built-in functions.

IV. RESULTS FOR BASELINE CONFIGURATION

This section presents the performance evaluation of the proposed MIMO-OFDM ISAC system under the baseline simulation configuration. The analysis is divided into two parts: communication performance and sensing performance. Communication results focus on the achieved data rates, modulation accuracy, and BER, while sensing results address target detection, localization, and range-Doppler estimation.

A. Communication

OFDM enables the efficient transmission of modulated signals over multiple orthogonal subcarriers. By employing higher-order modulation schemes, the system increases the number of bits transmitted per OFDM symbol, thereby enhancing the achievable data rate. In this configuration, 64-QAM modulation is used, allowing the encoding of six bits per symbol.

The use of multiple antennas at both the transmitter and receiver, in conjunction with a rich scattering environment, enables spatial multiplexing [20]. This technique permits the simultaneous transmission of multiple independent data streams over distinct spatial channels. In the simulated scenario, two independent data streams are transmitted from the

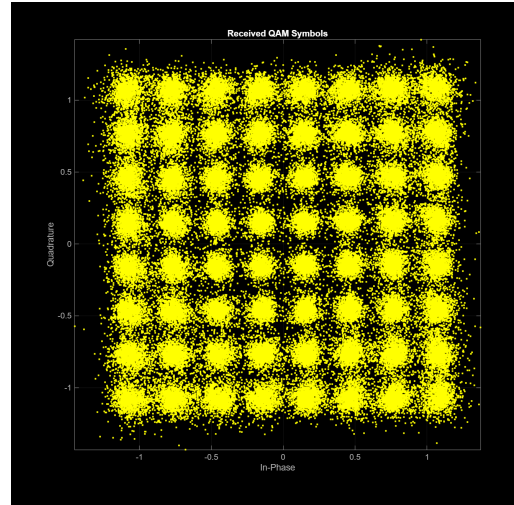


Fig. 5. Received constellation for a 64-QAM modulation scheme.

transmitter to the receiver using two spatial channels, which can theoretically double the throughput under ideal conditions.

Fig. 5 presents the received constellation for the 64-QAM modulation scheme. The distinct clustering of the constellation points reflects the system's ability to recover the transmitted information.

The average BER computed across all transmitted frames is 9.96×10^{-3} . This value, close to 10^{-2} , may not be sufficient for successful communications: according to common benchmarks, a BER on the order of 10^{-3} would be expected under favorable Signal-to-Noise Ratio (SNR) conditions. Therefore, the current setup does not reach the reliability levels anticipated for high-quality communication links.

A more favorable Bit Error Rate can be achieved by reducing the number of bits per symbol. For instance, when the modulation order is decreased from 64-QAM (6 bits per symbol) to 4-QAM (2 bits per symbol), the average BER improves to 8.76×10^{-4} . This reduction illustrates the classic trade-off between spectral efficiency and reliability: while higher-order constellations allow for increased data rates, they are more vulnerable to noise and channel impairments. Conversely, lower-order constellations sacrifice throughput but provide stronger resilience against errors.

B. Sensing

The collected radar data cube is processed to estimate the locations of scatterers within the propagation channel, initially filtering out static objects so that only moving targets are retained.

1) *Position Estimation:* The spatial distribution of the moving scatterers in the region of interest is visualized using a heatmap (Fig. 6). Two of the moving objects are detected at their expected positions, while the third target is not clearly identified in this representation. Additionally, a false alarm is observed in proximity to the receiver.

2) *Range and Velocity Estimation:* The range-Doppler response is used to analyze the target distances and Doppler characteristics. The range values correspond to the *sum range*,

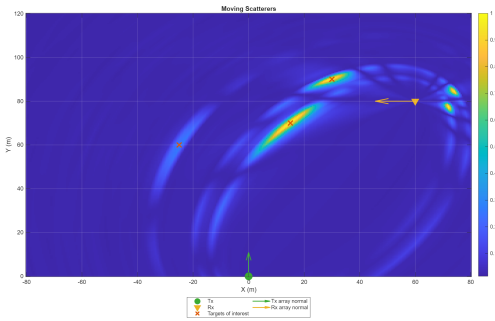


Fig. 6. Estimated positions of moving scatterers in the region of interest.

defined as the total propagation distance from the transmitter to the target and then to the receiver. The Doppler values represent the bistatic Doppler shift. Accurate target velocity estimation would require a multistatic radar configuration with multiple spatially distributed transmitters and/or receivers.

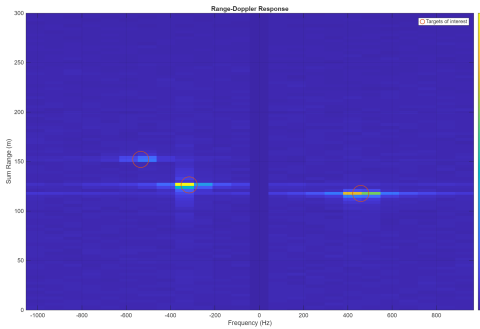


Fig. 7. Range–Doppler response showing target ranges and bistatic Doppler shifts.

Fig. 7 presents the range–Doppler response for the initial scenario. All three moving targets are correctly detected. One target exhibits a positive Doppler shift, indicating motion toward the radar, while the other two show negative shifts, indicating motion away. These observations are consistent with the velocity vectors shown in the initial scenario diagram (Fig. 2).

V. VARIATIONS ON SYSTEM PARAMETERS

After establishing the basic simulation setup, it is valuable to make adjustments to the system parameters to analyze the behavior of the system under different conditions. This section explores the impact of modifications to ... on the final results.

A. Array configuration

The number of transmit and receive antennas can be varied to evaluate the impact of array size and geometry on both communication capacity and sensing resolution. Larger arrays generally enhance angular resolution and improve direction-of-arrival (DoA) estimation, while also enabling more sophisticated beamforming strategies.

Simulation results confirm this trend across different configurations. For a compact setup with $N_{tx} = 4$ and $N_{rx} = 4$, the communication performance is noticeably degraded due to the limited beamforming gain. Increasing the transmit array size to $N_{tx} = 8$ while keeping $N_{rx} = 4$ (an asymmetric configuration) improves performance, although the unbalanced structure constrains angular diversity at the receiver. A balanced 8×8 MIMO system further enhances both throughput and sensing accuracy by doubling the receiver aperture. Scaling to a 16×16 or 20×20 configuration would be expected to yield significant improvements in interference suppression and angular resolution, thereby supporting high-capacity links. However, the obtained results do not fully reflect these intuitions, as the BER values remain similar to those achieved with smaller arrays, as summarized in Table III. This may be because the simulation parameters were fine-tuned for the 8×8 configuration, and further adjustments would be required to exploit the full potential of larger antenna arrays.

TABLE III
MEAN BER VALUES FOR DIFFERENT MIMO CONFIGURATIONS

Configuration	Mean BER
4×4	0.025959
8×4	0.012985
8×8	0.010046
16×16	0.023080
20×20	0.034340

An example of the degradation in sensing performance when reducing the number of antennas is shown in Fig. 8, where a 4×4 configuration is employed. With fewer antennas, the angular resolution and beamforming gain are diminished, impairing the system’s ability to resolve closely spaced targets and to detect distant ones. In addition, the overall scattered power is reduced compared to Fig. 7. While lowering N_{tx} simplifies the array design, it inevitably degrades sensing performance.

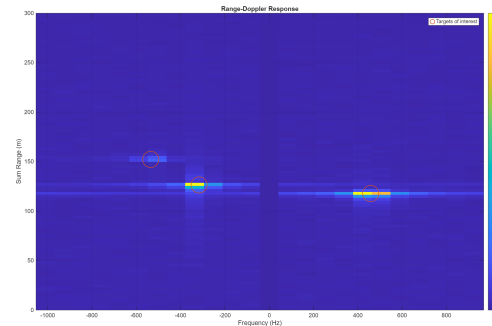


Fig. 8. Range-Doppler response for $N_{tx} = 4$.

B. Number of Subcarriers

The number of OFDM subcarriers has a direct impact on both bandwidth utilization and sensing resolution in the delay domain. Increasing the number of subcarriers enables finer range estimation, but at the expense of higher computational complexity and additional pilot overhead.

Conversely, reducing the number of OFDM subcarriers leads to larger subcarrier spacing for a fixed bandwidth, which can improve communication performance by enhancing robustness against Doppler shifts and Intersymbol Interference (ISI). This effect can be observed in Fig. 9, where the received constellation points are more tightly clustered compared to Fig. 5. In this case, the measured BER is approximately 3.56×10^{-3} (excluding the first frame, which exhibited abnormally poor performance).

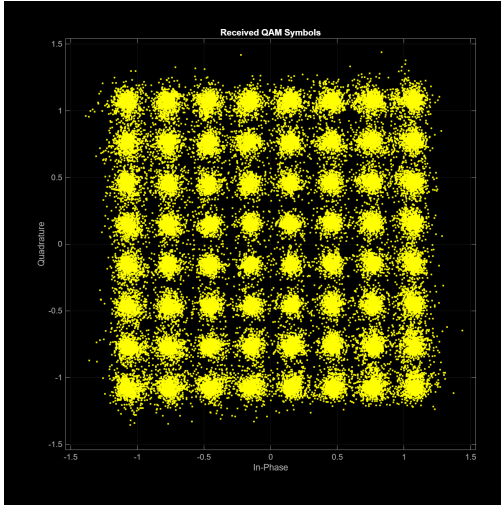


Fig. 9. Received constellation for a 64-QAM modulation scheme with 512 subcarriers.

However, this improvement in communication comes at the cost of sensing performance. A broader subcarrier spacing reduces frequency resolution, thereby degrading both range and Doppler resolution. This makes it more challenging to distinguish closely spaced targets or to accurately estimate high-velocity movements. As illustrated in Fig. 10, the scattered power decreases noticeably in comparison with Fig. 7.

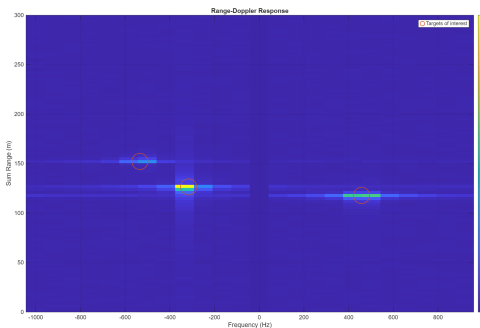


Fig. 10. Range–Doppler response for $N_{\text{sub}} = 512$.

On the other hand, increasing the number of subcarriers enhances sensing resolution but negatively affects communication performance. As shown in Fig. 11, the BER increases when $N_{\text{sub}} = 4096$, while the range–Doppler resolution, displayed in Fig. 12, is significantly improved.

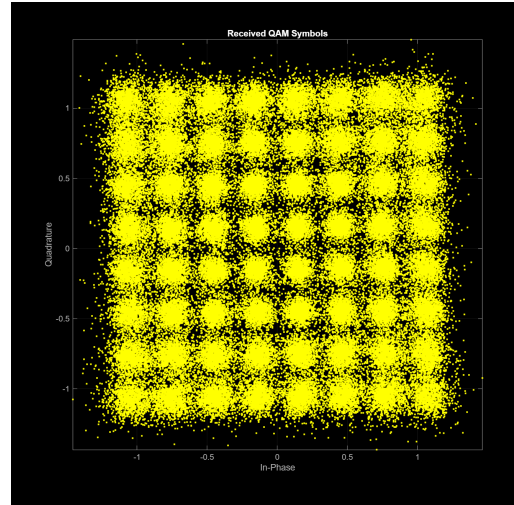


Fig. 11. Received constellation for a 64-QAM modulation scheme with 4096 subcarriers.

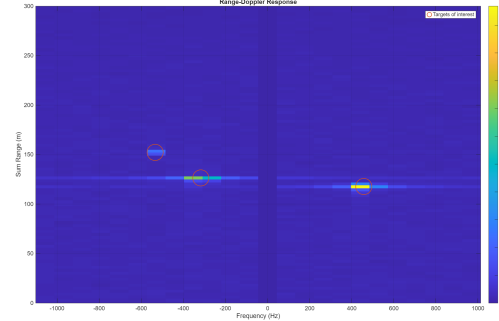


Fig. 12. Range–Doppler response for $N_{\text{sub}} = 4096$.

C. Data Streams

The number of parallel data streams determines the level of spatial multiplexing achievable in the system. Increasing the number of data streams enhances the overall throughput; however, it simultaneously exacerbates inter-stream interference and imposes stricter requirements on channel estimation accuracy, thereby affecting the reliability of sensing and communication performance.

In MIMO communications, the system provides $N_{\text{tx}} \times N_{\text{rx}}$ channels. Spatial multiplexing is feasible only under the condition

$$N_{\text{tx}} \geq N_{\text{rx}}. \quad (9)$$

To evaluate this effect, a 16×16 MIMO configuration was considered, with the number of data streams varied across three representative cases: 2, 4, and 8. The results indicate that higher numbers of data streams significantly degrade communication quality, as reflected in the BER performance and the corresponding constellation diagrams. In particular, distortions and symbol dispersion become increasingly severe with a larger number of data streams. Figure 13 illustrates the received constellation for the intermediate case of four streams under a 64-QAM modulation scheme.

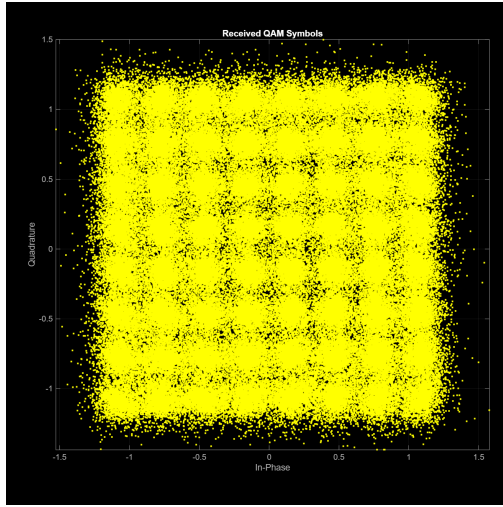


Fig. 13. Received constellation for a 64-QAM modulation scheme with 4 data streams.

Since sensing relies only on pilot information, no negative effect was observed across the tested configurations, making it less sensitive to the number of data streams than communications.

D. Target Modifications

The scenario can be modified by altering the positions and velocities of targets. These variations help assess the robustness of range-Doppler and angle estimation methods under different motion dynamics and geometrical configurations.

In this experiment, three additional targets were introduced to test the system under challenging conditions. First, a far-away target was added to assess the maximum detectable range. Second, a very fast-moving target was placed in the scene to evaluate Doppler resolution. Finally, a closely spaced target moving in parallel to another was considered to test angular and range resolution (see Fig. 14).

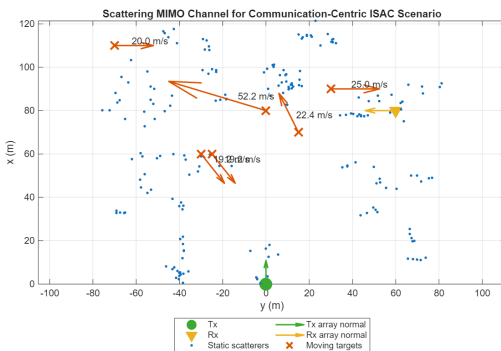


Fig. 14. ISAC scenario with additional moving targets.

The far-away target remained invisible in the heatmap (Fig. 15) and the range-Doppler map (Fig. 16), demonstrating the limits of the system in terms of maximum range. For the second target, the peak corresponding to this object is clearly

distinguishable in both graphs, although the range-Doppler response appears misaligned. Finally, the two closely spaced targets could not be separated, confirming the limited resolution in range and Doppler.

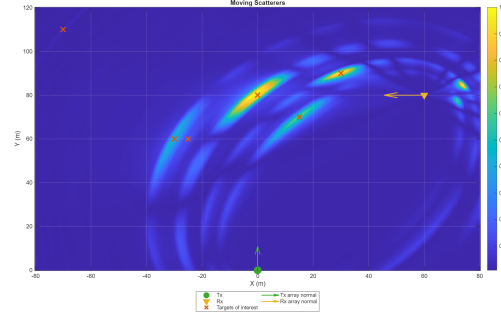


Fig. 15. Estimated positions of moving scatterers in the region of interest.

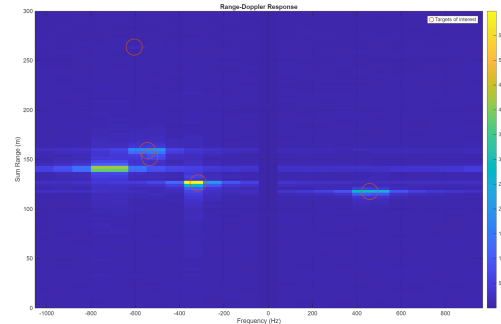


Fig. 16. Range-Doppler response showing target ranges and bistatic Doppler shifts.

On the communications side, the constellation diagram exhibits noticeable distortion, and the average BER across 24 frames worsened compared to the baseline case, likely due to the additional obstacles in the scenario that increase multipath propagation effects.

E. Pilot Configuration

Pilot design is essential to balance sensing accuracy and communication efficiency. Alternative pilot patterns, such as superimposed training, can reduce overhead and improve performance in low SNR regimes while still enabling accurate delay-Doppler estimation [18], [19].

In this work, different pilot allocation strategies were tested, including hexagonal and rectangular grids across the time-frequency plane. However, neither configuration produced satisfactory results: the hexagonal grid conflicted with the OFDM modulator constraint that requires distinct pilot positions per antenna, while the rectangular pattern introduced excessive interference and degraded channel estimation, likely due to a misconfiguration.

These outcomes suggest that implementing specific pilot modifications requires a deeper understanding of the underlying MATLAB custom functions, making it challenging to design and execute custom pilot patterns for channel updating.

F. Carrier Frequency, Bandwidth, and Subcarrier Spacing

Exploring multiple configurations of carrier frequency, bandwidth, and subcarrier spacing allows the evaluation of trade-offs between resolution, coverage, and hardware feasibility. Higher carrier frequencies (e.g., mmWave or THz) provide higher resolution but suffer from increased path loss and hardware constraints.

In OFDM-based ISAC systems, the bandwidth determines the range resolution according to

$$\delta_r = \frac{c}{2B}, \quad (10)$$

where B is the system bandwidth and c the speed of light. For instance, a 100 MHz bandwidth yields a range resolution of approximately 1.5 m, while extending to 2 GHz improves resolution to the order of centimeters.

The subcarrier spacing Δf controls the OFDM symbol duration ($T_{\text{sym}} \approx 1/\Delta f$) and thus the Doppler tolerance. Narrow subcarrier spacing improves robustness to multipath and increases the maximum unambiguous range, but results in longer symbols more susceptible to Doppler spread. Conversely, wider subcarrier spacing shortens the symbol duration, which is beneficial in high-mobility scenarios but reduces the maximum unambiguous range.

The carrier frequency f_c directly affects the wavelength, which determines angular resolution and Doppler sensitivity. At 6 GHz the wavelength is about 5 cm, whereas at 60 GHz it shrinks to 5 mm, enabling finer angular discrimination but also leading to higher propagation losses and stricter hardware requirements. In the Thz band, extremely high resolutions are possible, but practical deployment is limited by severe attenuation, atmospheric absorption, and hardware complexity.

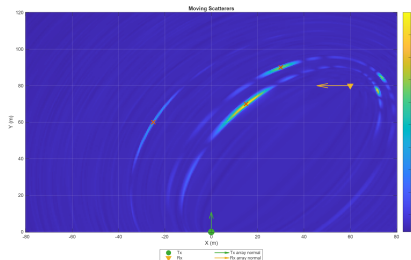


Fig. 17. Estimated positions of moving scatterers for $f_c = 12$ GHz and $\Delta f = 120$ kHz.

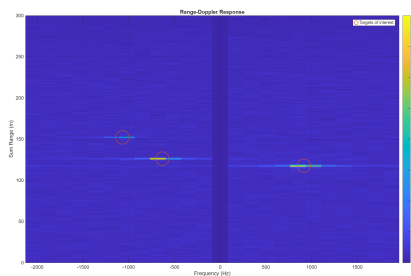


Fig. 18. Range-Doppler response for $f_c = 12$ GHz and $\Delta f = 120$ kHz.

To assess these trade-offs, a set of configurations based on 5G and emerging 6G numerologies has been defined [21], combining carrier frequencies at 6 GHz and 12 GHz with bandwidths ranging from 125 MHz to 1 GHz and subcarrier spacings of 60, 120, 480, and 960 kHz. This design space allows evaluating the sensitivity of both sensing and communication performance to frequency-domain parameters. Results highlight that while larger bandwidths and higher carrier frequencies enhance sensing resolution (see Figs. 17 and 18), they impose stringent demands on power consumption, system design, and computational time. Therefore, careful selection of numerology and carrier frequency is necessary to balance the requirements of simultaneous communications and sensing.

VI. CONCLUSIONS

This thesis has presented a simulation-based study of MIMO-OFDM configurations for ISAC. The analysis has revealed several key insights into the design of future 6G systems. First, there exist clear trade-offs in the choice of waveform parameters: increasing the number of OFDM subcarriers improves range resolution, but also raises computational complexity, while larger subcarrier spacings enhance Doppler resolution at the cost of reducing the maximum unambiguous range. Second, expanding the number of transmit and receive antennas strengthens sensing robustness and angular discrimination. However, the anticipated gains in communication performance were limited, primarily due to constraints in channel estimation and pilot design.

Another important observation concerns the differing sensitivity of communications and sensing. Communication reliability was found to degrade significantly when high levels of spatial multiplexing were employed, whereas sensing performance remained relatively stable, since it relies mainly on pilot information. This decoupling underscores the importance of jointly optimizing pilot allocation and data stream configurations to balance both functions. Finally, the study has shown that the system exhibits a built-in complexity: modifications of pilot configurations or attempts to adjust the signal-to-noise ratio did not always yield consistent improvements, as the results appear to be fine-tuned for the default scenario. Achieving better outcomes often required simultaneous changes in multiple parameters, and predicting the most effective combinations proved difficult.

In summary, MIMO-OFDM provides a flexible and well-understood baseline for ISAC, benefiting from its maturity in existing wireless standards. Nevertheless, fully realizing its potential in 6G will demand more advanced pilot structures, scalable antenna processing, and possibly machine learning-based approaches for robust channel and target estimation. Future research directions include extending the simulation framework to THz-band scenarios and exploring alternative pilot designs.

REFERENCES

- [1] D. K. Pin Tan, J. He, Y. Li, A. Bayesteh, Y. Chen, P. Zhu, and W. Tong, "Integrated Sensing and Communication in 6G: Motivations, Use Cases, Requirements, Challenges and Future Directions," in *2021 1st IEEE International Online Symposium on Joint Communications*

- & Sensing (JC&S). Dresden, Germany: IEEE, Feb. 2021, pp. 1–6. [Online]. Available: <https://ieeexplore.ieee.org/document/9376324/>
- [2] T. Gan, S. Dang, X. Li, and Z. Zhang, “Integrated Sensing and Communications for 6G: Prospects and Challenges of Using THz Radios,” in *2024 IEEE Wireless Communications and Networking Conference (WCNC)*. Dubai, United Arab Emirates: IEEE, Apr. 2024, pp. 1–6. [Online]. Available: <https://ieeexplore.ieee.org/document/10570679/>
- [3] W. Zhou, R. Zhang, G. Chen, and W. Wu, “Integrated Sensing and Communication Waveform Design: A Survey,” *IEEE Open Journal of the Communications Society*, vol. 3, pp. 1930–1949, 2022. [Online]. Available: <https://ieeexplore.ieee.org/document/9924202/>
- [4] H. Sampath, S. Talwar, J. Tellado, V. Erceg, and A. Paulraj, “A fourth-generation MIMO-OFDM broadband wireless system: design, performance, and field trial results,” *IEEE Communications Magazine*, vol. 40, no. 9, pp. 143–149, Sep. 2002. [Online]. Available: <https://ieeexplore.ieee.org/document/1031841>
- [5] C. Dubuc, D. Starks, T. Creasy, and Y. Hou, “A MIMO-OFDM prototype for next-generation wireless WANs,” *IEEE Communications Magazine*, vol. 42, no. 12, pp. 82–87, Dec. 2004. [Online]. Available: <https://ieeexplore.ieee.org/document/1367559>
- [6] IEEE Standards Association, “802.16a-2003 IEEE Standard for Local and Metropolitan Area Networks,” Standard, 2003. [Online]. Available: <https://standards.ieee.org/ieee/802.16a/3114/>
- [7] K. Sharma, T. Kumar, and K. Ramesh, “Performance study of OFDM over multipath fading channels for next wireless communications,” *International Journal of Applied Engineering Research*, vol. 12, pp. 10 205–10 210, 01 2017.
- [8] T.-L. Tung, K. Yao, and R. Hudson, “Channel estimation and adaptive power allocation for performance and capacity improvement of multiple-antenna OFDM systems,” in *2001 IEEE Third Workshop on Signal Processing Advances in Wireless Communications (SPAWC’01). Workshop Proceedings (Cat. No.01EX471)*, Mar. 2001, pp. 82–85. [Online]. Available: <https://ieeexplore.ieee.org/document/923849>
- [9] I. Barhumi, G. Leus, and M. Moonen, “Optimal training design for MIMO OFDM systems in mobile wireless channels,” *IEEE Transactions on Signal Processing*, vol. 51, no. 6, pp. 1615–1624, Jun. 2003. [Online]. Available: <https://ieeexplore.ieee.org/document/1200150>
- [10] A. Mody and G. Stuber, “Receiver implementation for a MIMO OFDM system,” in *IEEE Global Telecommunications Conference, 2002. GLOBECOM ’02*, vol. 1, Nov. 2002, pp. 716–720 vol.1. [Online]. Available: <https://ieeexplore.ieee.org/document/1188172>
- [11] T. MathWorks Inc., “Integrated Sensing and Communication II: Communication-Centric Approach Using MIMO-OFDM,” 2024. [Online]. Available: <https://shorturl.at/jXeuo>
- [12] O. González Fresno, “oscgf/mimo-ofdm-isac,” 2025. [Online]. Available: <https://github.com/oscgf/mimo-ofdm-isac>
- [13] T. MathWorks Inc., “Decide When to Use parfor - MATLAB & Simulink.” [Online]. Available: <https://es.mathworks.com/help/parallel-computing/decide-when-to-use-parfor.html>
- [14] —, “Run MATLAB Functions on a GPU - MATLAB & Simulink.” [Online]. Available: <https://es.mathworks.com/help/parallel-computing/run-matlab-functions-on-a-gpu.html>
- [15] A. Stamoulis, S. Diggavi, and N. Al-Dhahir, “Intercarrier interference in MIMO OFDM,” *IEEE Transactions on Signal Processing*, vol. 50, no. 10, pp. 2451–2464, Oct. 2002. [Online]. Available: <https://ieeexplore.ieee.org/document/1033676>
- [16] W. Henkel, G. Taubock, P. Odling, P. Borjesson, and N. Petersson, “The cyclic prefix of OFDM/DMT - an analysis,” in *2002 International Zurich Seminar on Broadband Communications Access - Transmission - Networking (Cat. No.02TH8599)*, Feb. 2002, pp. 22–22. [Online]. Available: <https://ieeexplore.ieee.org/document/991762/>
- [17] Y. L. Sit, B. Nuss, and T. Zwick, “On Mutual Interference Cancellation in a MIMO OFDM Multiuser Radar-Communication Network,” *IEEE Transactions on Vehicular Technology*, vol. 67, no. 4, pp. 3339–3348, Apr. 2018. [Online]. Available: <https://ieeexplore.ieee.org/document/8169087>
- [18] L. M.-M. Suárez, K. Chen-Hu, M. J. F.-G. García, and A. G. Armada, “Robust Integrated Sensing and Communications in Delay-Doppler Domain Using Superimposed Training,” in *2023 IEEE Globecom Workshops (GC Wkshps)*. Kuala Lumpur, Malaysia: IEEE, Dec. 2023, p. 6. [Online]. Available: <https://ieeexplore.ieee.org/document/10464932/>
- [19] Y. Wu, C. Han, and Z. Chen, “DFT-Spread Orthogonal Time Frequency Space System With Superimposed Pilots for Terahertz Integrated Sensing and Communication,” *IEEE Transactions on Wireless Communications*, vol. 22, no. 11, pp. 7361–7376, Nov. 2023. [Online]. Available: <https://ieeexplore.ieee.org/document/10061469>
- [20] H. Bolcskei, D. Gesbert, and A. Paulraj, “On the capacity of OFDM-based spatial multiplexing systems,” *IEEE Transactions on Communications*, vol. 50, no. 2, pp. 225–234, Feb. 2002. [Online]. Available: <https://ieeexplore.ieee.org/document/983319>
- [21] 3GPP, “NR; User Equipment (UE) radio transmission and reception; Part 1: Range 1 Standalone,” 3rd Generation Partnership Project (3GPP), Technical Specification (TS) 38.101-1, 01 2025, version 19.0.0. [Online]. Available: <https://portal.3gpp.org/desktopmodules/Specifications/SpecificationDetails.aspx?specificationId=3283>